Crossover from the Rouse to the Entangled Polymer Melt Regime: Signals from Long, Detailed Atomistic Molecular Dynamics Simulations, Supported by Rheological Experiments

V. A. Harmandaris,[†,‡] V. G. Mavrantzas,[*,†] D. N. Theodorou,[†,‡] M. Kröger,[§,⊥] J. Ramírez,[§] H. C. Öttinger,[§] and D. Vlassopoulos[||]

Institute of Chemical Engineering and High-Temperature Chemical Processes, (ICE/HT-FORTH), GR 26500, Patras, Greece, Department of Chemical Engineering, University of Patras, GR 26500 Patras, Greece, Department of Materials, Institute of Polymers, ETH Zürich, CH-8092 Zürich, Switzerland, Swiss Rheocenter, CH-8092 Zürich, Switzerland, Institut für Theoretische Physik, Technische Universität Berlin, D-10623 Berlin, Germany, and Institute of Electronic Structure and Laser (IESL-FORTH), P.O. Box 1527, Heraklion 71110, Crete, Greece

Received January 7, 2002; Revised Manuscript Received November 15, 2002

ABSTRACT: Results are presented from 300 ns long atomistic molecular dynamics (MD) simulations of polyethylene (PE) melts, ranging in molecular length from C_{78} to C_{250}. Above C_{156}, the self-diffusion coefficient D is seen to exhibit a clear change in its power-law dependence on the molecular weight (M), significantly deviating from a Rouse (where $D \sim M^{-1}$) toward a reptation-like (where $D \sim M^{-2.4}$) behavior. The mean-square displacement (msd) of chain segments and the dynamic structure factor is also calculated and the crossover from the Rouse to entangled behavior is again observed above C_{156}. A novel strategy is also developed for projecting atomistic chain configurations to their primitive paths and thereby mapping simulation trajectories onto the reptation model. Results for the friction factor ζ, the zero-shear rate viscosity η_0 and the self-diffusion coefficient D are found to be internally consistent and in agreement with experimental rheological data.

I. Introduction

The dynamics of polymer melts as a function of their molecular length has attracted considerable attention in the last years. Experimentally, a clear change is seen in the mechanism of chain dynamics when the molecular weight (M) of the melt exceeds a characteristic polymer-dependent value, M_e.[1] The slope, in logarithmic coordinates, of the self-diffusion coefficient D as a function of molecular length changes from -1 to -2, whereas the exponent in the power-law dependence of the zero-shear rate viscosity η_0 on M goes from 1 to 3.4. Traditionally, this change or crossover has been attributed to the emergence of topological constraints that hinder the overall chain motion.[1,2]

The dynamics of short polymer melts ($M < M_e$) is well described by the Rouse model,[2,3] wherein a chain is envisioned as a set of Brownian particles connected by harmonic springs. The Rouse model is formulated in terms of three parameters: the number of beads N_k, the length of the Kuhn segment b_k, and the monomeric friction coefficient ζ. A modified Rouse model that incorporates local stiffness, the semiflexible chain model,[4] shows a better agreement with experimental results mainly for motion over shorter lengths.[4] For melts with $M > M_e$, a theory that describes polymer dynamics quite successfully is reptation. This theory postulates that the motion of an individual chain is restricted by the surrounding chains within a tube defined by the overall chain contour or primitive path. During the lifetime of this tube, any lateral motion of the chain is quenched. Reptation theory is formulated in terms of four parameters: N_k, b_k, ζ, and the entanglement spacing (or, alternatively, the tube diameter) α. At the same time other theories predict the dynamics of entangled polymer melts without incorporating the reptation hypothesis such as the Ronca model,[5] the generalized Rouse model,[6] and the des Cloizeau approach.[7] A different approach was followed by Schweizer[8] through the development of the mode−mode coupling theory for polymers.

Experimentally, microscopic signals of reptation dynamics have been evidenced from various measurements. Perkins et al. first reported the tubelike motion of a single DNA chain in an entangled solution using fluorescence microscopy.[9] Neutron spin echo (NSE) experiments in the time range $t = 0.3-175$ ns[10−14] were consistently analyzed in the context of reptation theory. In more detail, the single chain dynamic structure factor $S(q,t)$ was calculated and compared with theoretical expressions from various models.[5,6,15] Reptation theory was documented as the only one that provides a consistent description of all NSE data.[10] More recently, double-quantum nuclear magnetic resonance (DQ NMR) experiments, probing the translational motion of polybutadiene (PB) chains, gave scaling laws consistent with the reptation model.[16]

Besides experiments, molecular simulations have also been used to probe chain dynamics and relaxation in polymer melts. Among these, molecular dynamics (MD) and nonequilibrium molecular dynamics (NEMD) have been dominant. NEMD simulations of steady shear flow, in particular, lead directly to the calculation of the shear

* To whom correspondence should be addressed at ICE/HT-FORTH. E-mail: vlasis@iceht.forth.gr. Telephone: +30-2-610-965 214. Fax: +30-2-610-965 223.
[†] Institute of Chemical Engineering and High-Temperature Chemical Processes (ICE/HT-FORTH).
[‡] University of Patras, GR 26500 Patras, Greece
[§] Department of Materials, Institute of Polymers, ETH Zürich, and Swiss Rheocenter.
[⊥] Technische Universität Berlin.
[||] Institute of Electronic Structure and Laser (IESL-FORTH).

10.1021/ma020009g CCC: $25.00
Published on Web 01/29/2003

viscosity.[17] Signal-to-noise ratio usually necessitates that NEMD be performed at very high flow rates, deeply in the nonlinear regime. Furthermore, the attainment of steady-state conditions through a NEMD run initiated at an equilibrium configuration becomes problematic, since the longest relaxation time of the molecules may significantly exceed the duration of the simulation. Alternatively, one can obtain viscosity in the linear regime in the course of equilibrium MD simulations, following the Green−Kubo formalism.[18]

The most challenging task in all polymer MD simulations is the long simulation times required to track the evolution of the system, particularly at high molecular lengths. Understandably, detailed atomistic dynamic simulations of melts higher than about C_{120} have never been performed.[19−21] All systems studied with atomistic MD up to now are below M_e and exhibit the well-known Rouse-like behavior, at least for the overall chain dynamics.

To study entangled systems, coarse-grained models have been employed, since the pioneering MD work of Kremer and Grest.[22] Recenlty, Pütz et al.[23] presented evidence for a passage from Rouse to reptation dynamics based on the slope of the segmental mean square displacement (msd) in different time regimes following the scalings of the reptation model. The reptation scalings for the diffusion and the msd were also confirmed by Smith et al. through MD simulations with the simple freely jointed tangent hard sphere or pearl necklace model.[24]

NEMD simulations of flexible FENE chains in a planar Couette flow have also been reported by Kröger and Hess.[25] By directly calculating η_0 as a function of chain length, a critical M was observed at a chain length around 100 beads per chain, where a clear change in the power-law dependence of the viscous properties occurred.

At the same time, Monte Carlo (MC) simulations using lattice and off-lattice coarse-grained models have been developed. Pakula and Geyler presented results from MC simulations of a fully occupied cubic lattice,[26] where chains are moving through a cooperative rearrangement mechanism involving replacement of chain elements (beads) in systems where space is fully filled. For the longer chains, the molecular weight dependence of the self-diffusion coefficient D was found to coincide with the prediction of the reptation theory; regarding the msd of segments, however, only small deviations were observed from the Rouse behavior. More recently, Haire et al. have conducted MC simulations with a similar model incorporating an algorithm which allows several beads to move together.[27] For a system consisting of chains with 200 beads long, their results about the evolution of the msd of segments in time show that the power law exponent in the intermediate regime is 0.36 (as compared to the value of 0.25, predicted by the reptation theory). The same slope had also been observed in earlier dynamic MC simulations with the same system by employing the bond fluctuation model.[28] The bond fluctuation model has also been used in a later study by Kreer et al. to probe the crossover from a Rouse to a reptation-like regime in chain systems up to 512 beads long.[29] A gradual crossover transition was documented in their simulations where the power-law exponent in the intermediate regime quantifying the msd of segments with time was seen to be a decreasing function of chain length.

A different simulation procedure has been followed by Padding and Briels based on tracking bond crossings in coarse-grained Brownian dynamics (BD) simulations of entangled systems.[30] Calculated diffusion coefficients and their dependence on molecular length were found to be consistent with the predictions of the classical reptation theory.

This paper is organized as follows. Section II presents the molecular model used with a brief description of the multiple time step integration method adopted. The experimental part of our work is presented in section III. Section IV explains the hierarchical methodology followed and shows the mapping of the atomistic results onto the Rouse and the reptation model. Results from the atomistic MD simulations for the segment displacements, chain self-diffusivity, single-chain intermediate dynamic structure factor, friction factor, and zero-shear rate viscosity are presented in section V and compared directly against recently obtained experimental data. Finally the major conclusions of the present work and current efforts are summarized in section VI.

II. Molecular Model: Systems Studied

A united-atom description is used in the present work, with methylene and methyl groups considered as a single Lennard-Jones interaction site. Nonbonded interactions are described by a Lennard-Jones potential of the form

$$V_{\mathrm{LJ}}(r) = 4\epsilon\left[\left(\frac{\sigma}{r}\right)^{12} - \left(\frac{\sigma}{r}\right)^{6}\right] \tag{1}$$

with $\epsilon = 0.098$ kcal/mol and $\sigma = 3.94$ Å. $V_{\mathrm{LJ}}(r)$ describes all intermolecular site−site interactions as well as intramolecular interactions between sites separated by more than three bonds. A potential cutoff distance of 9.062 Å is used. Attractive tail contributions are dealt with through direct integration.[31] A bond-bending potential of the form[32]

$$V_{\mathrm{bending}}(\theta) = \frac{1}{2}k_\theta(\theta - \theta_0)^2 \tag{2}$$

is also used for every skeletal bond angle θ, with $k_\theta = 115.2$ kcal mol^{-1} rad^{-2} and $\theta_0 = 112°$. Associated with each dihedral angle ϕ is a torsional potential of the form[33]

$$V_{torsional}(\phi) = c_0 + c_1\cos\phi + c_2(\cos\phi)^2 + c_3(\cos\phi)^3 + c_4(\cos\phi)^4 + c_5(\cos\phi)^5 \tag{3}$$

with $c_0 = 2.217$, $c_1 = 2.905$, $c_2 = -3.135$, $c_3 = -0.731$, $c_4 = 6.271$, and $c_5 = -7.527$ in kcal/mol.

Adjacent methyl and methylene groups are maintained at a fixed distance $l = 1.54$ Å using the SHAKE method.[34,35]

The equations of motion are integrated with a velocity Verlet method. To speed up the MD simulations, a multiple time step (MTS) algorithm is used, namely the reversible reference system propagator algorithm (rRESPA), first proposed by Tuckerman et al. and Martyna et al.[36,37] This reversible algorithm is based on a separation of the Liouville operator into two different operators. The first operator describes the motion of fast degrees of freedom, which is integrated with a small time step dt. The second operator includes more slowly varying interactions, whose evolution is

tracked with a larger time step $Dt = i\,dt$, where i is an integer. Indeed, polymers exhibit a wide spectrum of time scales, extending from fast local modes (involving bond stretching, bond-angle bending and torsional vibrations around skeletal bonds) to very slow modes (describing motion at the level of entire chains). In our simulations, the slowly varying part of the Liouville operator includes mainly the intermolecular and intramolecular nonbonded LJ interactions. Bond bending and torsional potentials are included in the fast varying part. Consequently, the number of computationally expensive LJ force evaluations, which is usually the most time-consuming part in an MD simulation, is significantly reduced for a given overall simulation time. To control the temperature a variation of the rRESPA scheme, the XI−RESPA algorithm that incorporates the Nosé−Hoover thermostat, is used.[37] Using rRESPA, we have been able to speed up the calculations involved in a typical *NVT* MD run by 2−5 times over the conventional single-step MD algorithm. In all simulations reported in the present study, the smaller time step dt was taken equal to 2 fs and the larger time step Dt equal to $5dt$, i.e. 10 fs. The overall simulation time ranged from 100 to 300 ns depending on the molecular length of the system studied.

The 20-chain C_{156}, 20-chain C_{180}, 25-chain C_{200}, and 16-chain C_{250} PE melts have been simulated, all characterized by uniform chain length distributions with a polydispersity index I around 1.05. All MD simulations have been conducted in the canonical (NVT) statistical ensemble, at $T = 450$ K and $P = 1$ atm. Initial configurations were obtained from end-bridging Monte Carlo (EBMC) simulations[38] of the same model systems at the same T and P, corresponding to densities ρ equal to 0.800, 0.800, 0.795, 0.790, and 0.775 g/cm^3, for the C_{250}, C_{200}, C_{180}, C_{156}, and C_{78} PE melts, respectively.

III. Rheological Measurements

The results obtained from the *NVT* MD simulations conducted here were compared against available experimental data reported in the literature as well as against new rheological measurements carried out in the course of this work. To this end, several linear polyethylene samples ranging in molecular weight M between 950 and 111500 were obtained from Polymer Source. They were prepared from anionically synthesized 1,4-polybutadiene, which was subsequently hydrogenated. The polymers were thoroughly characterized and their polydispersities were found to satisfy $M_w/M_n \leq 1.08$.

With these samples, rheological measurements were carried out in strain- and stress-controlled rheometers from Rheometric Scientific (ARES 2KFRTN1 and DSR-200, respectively). They involved dynamic linear frequency and/or steady shear rate or stress sweeps at 180 °C under equilibration conditions (checked via time sweeps) and in the presence of nitrogen atmosphere to reduce the risk of degradation. From these experiments, the zero shear viscosity η_0 was readily obtained. Note that in some cases, limitation in the torque resolution did not allow direct access to η_0, which was then determined by fitting the relevant rheogram to the Carreau model.

IV. Simulation Methodology

To overcome the problem of long relaxation times present in atomistic MD simulations of high polymer melts and get at their rheological properties, hierarchical approaches must be adopted. Recently, we have presented a three-stage approach,[19,39] whereby the dynamic properties of polymer melts are calculated through (a) exhaustive EBMC simulations[38] to equilibrate the melts at all length scales, (b) atomistic MD simulations accumulating a large number of dynamical trajectories,[19] and (c) mapping of these trajectories onto a mesoscopic model. This approach has enabled the prediction of the linear viscoelastic properties of polymer melts of length up to C_{117} and narrow M distribution. The Rouse model was seen to describe the overall chain dynamics of these systems quite accurately, provided the chain length exceeded about C_{60}.

In this paper, this hierarchical approach is extended to melts of longer molecules, up to C_{250}. Key to the dynamic simulations is the multiple time step (MTS) algorithm, which allows us to track the evolution of the systems for very long times, up to 300 ns. We show that the dynamics of systems longer than about C_{156} cannot be mapped onto the Rouse model. In contrast, the reptation model offers a much more faithful representation of the dynamics of the simulated melts. This is the first time that convincing evidence for the crossover from a Rouse to a reptation-like behavior is documented, directly from detailed atomistic MD simulations that are free of any limitations of a coarse-grained molecular model. Also presented for the first time is a self-consistent, reliable procedure for calculating the tube diameter and the zero-shear rate viscosity from such simulations.

A property that can be obtained directly from the atomistic MD simulations (without any need for mapping atomistic trajectories onto a mesoscopic model) and compared immediately with experimental results is the self-diffusion coefficient D. D is calculated from the linear part of the msd of the chains centers-of-mass as a function of time, according to the Einstein relation. In contrast to D, the rest of the dynamic and rheological properties (such as the monomeric friction factor ζ, the zero-shear rate viscosity η_0 and the spectrum of relaxation times) are best obtained after mapping the atomistic MD trajectories onto a mesoscopic theoretical model. The most popular models are the Rouse model for $M < M_e$ and the reptation theory for $M > M_e$.

A. Mapping onto the Rouse Model. The Rouse model is formulated in terms of the normal coordinates or modes $\mathbf{X}_p$, $p = 0, 1, 2, \ldots, N-1$, each of which is capable of independent motion. On the basis of this, the Rouse model expression for the time autocorrelation function $\langle \mathbf{X}_p(t)\cdot\mathbf{X}_p(0)\rangle$ is[2]

$$\langle \mathbf{X}_p(t)\cdot\mathbf{X}_p(0)\rangle = \frac{k_B T}{k_p}\exp\left(-\frac{t}{\tau_p}\right) = \frac{Nb^2}{6\pi^2}\frac{1}{p^2}\exp\left(-\frac{p^2 t}{\tau_R}\right) \quad (4)$$

where τ_R is the maximum (Rouse) relaxation time:

$$\tau_R = \frac{\zeta N^2 b^2}{3\pi^2 k_B T} \quad \text{and} \quad \tau_p = \frac{\tau_R}{p^2}. \quad (5)$$

The monomeric friction coefficient ζ can be calculated directly from D through

$$\zeta = \frac{k_B T}{ND} \quad (6)$$

and the zero-shear rate viscosity η_0 through

$$\eta_0 = \frac{\rho R T}{36M}\frac{\langle R^2\rangle}{D} \tag{7}$$

where ρ is the mass density of the melt and $\langle R^2\rangle$ the equilibrium mean-square chain end-to-end distance.

Of interest is also the prediction of the Rouse model for the msd of the chain segments, $\phi(n,t)$, defined through

$$\phi(n,t) \equiv \langle(\mathbf{R}(n,t) - \mathbf{R}(n,0))^2\rangle. \tag{8}$$

This is calculated to be (see ref 2, p 133, eq 4.III.6):

$$\phi(n,t) = 6Dt + \frac{4\langle R^2\rangle}{\pi^2}\sum_{p=1}^{\infty}\frac{1}{p^2}\cos\left(\frac{p\pi n}{N}\right)^2[1 - \exp(-tp^2/\tau_R)] \tag{9}$$

For very short times ($t < \tau_R$), $\phi(n,t)$ is dominated by the terms with large p and $\phi(n,t)$ scales as $t^{1/2}$. On the other hand, for longer times ($t \gg \tau_R$), the second term in eq 9 may be neglected and $\phi(n,t)$ scales as t.

The Rouse model results into an analytic expression also for the single-chain intermediate dynamic structure factor, $S(q,t)$, a quantity which is experimentally accessible. $S(q,t)$ is defined as

$$S(q,t) \equiv \sum_{nm}\langle\exp[i\mathbf{q}\cdot\mathbf{R}_{nm}(t)]\rangle \tag{10}$$

where $\mathbf{q}$ is the scattering vector and n, m denote atoms belonging to the same chain. In eq 10, $\mathbf{R}_{nm}(t)$ is a displacement vector between chain segments n, m defined as

$$\mathbf{R}_{nm}(t) \equiv \mathbf{R}(n,t) - \mathbf{R}(m,0) \tag{11}$$

with $\mathbf{R}(n,t)$ denoting the position vector of the chain segment n at time t and $\mathbf{R}(m,0)$ the position vector of the chain segment m at time 0. For an isotropic (melt) sample, eq 10 reduces to[2]

$$S(q,t) = \sum_{nm}\langle\sin[qR_{nm}(t)]/qR_{nm}(t)\rangle \tag{12}$$

where $R_{nm}(t)$ is the magnitude of $\mathbf{R}_{nm}(t)$.

Of interest is the normalized single-chain intermediate coherent dynamic structure factor, which is measured directly in the neutron spin echo (NSE) experiments. This is defined as

$$S'(q,t) = \frac{S(q,t)}{S(q,0)} = \frac{\sum_{nm}\langle\sin[qR_{nm}(t)]/qR_{nm}(t)\rangle}{\sum_{nm}\langle\sin[qR_{nm}(0)]/qR_{nm}(0)\rangle} \tag{13}$$

Equation 13 can also be used to extract $S'(q,t)$ directly from the MD simulations by recording the time correlation function of chain segments n, m.

By further assuming that segmental displacements follow a Gaussian distribution, one observes that the single-chain dynamic structure factor simplifies to

$$S(q,t) \equiv \sum_{nm}\exp\left[-\frac{q^2}{6}\phi(n,m;t)\right] \tag{14}$$

where $\phi(n,m;t)$ is the time correlation function of chain segments n, m:

$$\phi(n,m;t) \equiv \langle(\mathbf{R}(n,t) - \mathbf{R}(m,0))^2\rangle \tag{15}$$

Further analysis requires the explicit calculation of the quantity $\phi(n,m;t)$. For the finite (i.e., the discrete) Rouse model, such a derivation is carried out in Appendix A. By combining the resulting expression, eq A.6, with eq 14, we find that

$$S(q,t) = \frac{1}{N_k}\exp[-q^2Dt]\sum_{n,m}^{N_k}\exp\left\{-\frac{q^2b_k^2}{12N_k}\sum_{p=1}^{N_k-1}\frac{1}{\sin^2\left(\frac{p\pi}{2N_k}\right)}\left[\cos\left(\frac{p\pi(m-{}^1/_2)}{N_k}\right) - \cos\left(\frac{p\pi(n-{}^1/_2)}{N_k}\right)\right]^2 - \frac{q^2b_k^2}{6N_k}\sum_{p=1}^{N_k}\frac{1}{\sin^2\left(\frac{p\pi}{2N_k}\right)}\cos\left(\frac{p\pi(n-{}^1/_2)}{N_k}\right)\cos\left(\frac{p\pi(m-{}^1/_2)}{N_k}\right)\left[1 - \exp\left(-\frac{t}{\tau_p}\right)\right]\right\} \tag{16}$$

where N_k denotes the number of statistical segments in the chain, b_k the statistical segment length, and D the center-of-mass diffusion coefficient.

In the high N limit, the following approximations apply: $i - {}^1/_2 \cong i$ and $\sin^2(p\pi/2N_k) \cong (p\pi/2N_k)^2$ (for $p \ll N_k$). With the help of these, the following well-known expression for the dynamic structure factor $S(q,t)$ is derived,[2] corresponding to the continuous Rouse model:

$$S(q,t) = \frac{1}{N_k}\exp[-q^2Dt]\sum_{n,m}^{N_k}\exp\left\{-\frac{q^2b_k^2}{6}|n-m| - \frac{2q^2N_kb_k^2}{3\pi^2}\sum_{p=1}^{N_k}\frac{1}{p^2}\cos\left(\frac{p\pi n}{N_k}\right)\cos\left(\frac{p\pi m}{N_k}\right)\left[1 - \exp\left(-\frac{t}{\tau_p}\right)\right]\right\} \tag{17}$$

For $q\langle R^2\rangle \ll 1$, only the overall diffusion of the chains is monitored and, then, $S(q,t) = \exp(-q^2Dt)$.

Recently, a modification of the Rouse model, the semiflexible chain model (SFCM), was proposed by Harnau et al.[4] that incorporates local chain stiffness effects. According to the SCFM, the Rouse mode relaxation times are given by

$$\tau^b{}_p = \frac{\tau_R}{p^2 + \alpha_b p^4} = \frac{\tau_R}{p^2 + \frac{\pi^2C_\infty^2}{4N^2\sin^4(\theta/2)}p^4} \tag{18}$$

where the term proportional to p^4 is the correction to the Rouse model due to rigidity effects, and C_∞ denotes the characteristic ratio at infinite chain length. For the smaller normal modes, the corrected relaxation times

τ^b_p's are almost equal to τ_p's; for the higher mode numbers, however, the τ^b_p's decrease faster than the corresponding τ_p's. In this case, the single-chain dynamic structure factor is calculated by using again eq 16 but with the relaxation times τ_p taken from eq 18.

B. Mapping onto the Reptation Model. Mapping atomistic MD data onto the reptation model is a subtle task, because reptation theory has been formulated in terms of chain primitive paths, through an appropriate coarse-graining of the atomistic chain configurations. Carrying out such a coarse-graining or mapping is not an easy task. It has been addressed only very recently by Kröger et al.,[40] through a projection operation involving a single parameter ξ, governing the stiffness of the chain in the coarse-grained (primitive path) representation. The parameter ξ is mathematically defined as the ratio of the constants of two types of Hookean springs: The first type connects adjacent beads within the projected primitive path, and the second type connects the projected beads of the primitive path with the corresponding atomistic units. The coordinates of the primitive path are obtained by minimizing the total mechanical energy of the springs. The parameter ξ of the projection may be interpreted in several ways. In general, ξ controls the Kuhn length, contour length, and the width or tube diameter of the primitive path, which defines the number of "entanglements" in the Doi−Edwards[2] terminology. Stiffening of the primitive path comes together with a shrinking of the contour length, but usually one wishes to fix the contour length as an independent parameter of the projection. According to Kröger et al.,[40] this may be achieved by further introducing a Maxwellian demon (with fixed strength according to a given temperature) pulling at the ends of the primitive path in the direction of the end segments while preserving the contour length by further adjusting ξ. However, in this case, the resulting system of equations becomes nonlinear and this increases the computational cost. In the calculations reported here, the fixed-end version of the mapping of the atomistic chains onto their primitive paths was followed.

In general, different values of ξ lead to different parametrizations, i.e., to different primitive paths and, consequently, to different degrees of entanglement. Once a value for ξ has been chosen, the primitive path is fully defined and its contour length L fully specified. This allows calculating the tube diameter α through the following equation of reptation theory:

$$L\alpha = \langle R^2 \rangle \tag{19}$$

with the value $\langle R^2 \rangle$ borrowed from the atomistic simulations. Further, once the projection from the atomistic to the primitive path representation has been made, the msd of the primitive path points, $\phi(s,s;t)$, defined as

$$\phi(s,s;t) \equiv \langle (\mathbf{R}(s,t) - \mathbf{R}(s,0))^2 \rangle \tag{20}$$

can be easily calculated. In eq 20, $\mathbf{R}(s,t)$ is the position vector of the *primitive* segment at contour length s at time t and $\mathbf{R}(s,0)$ the position vector of the *primitive* segment at contour length s at time 0. According to reptation theory (see ref 2, p 200, eq 6.36)

$$\phi(s,s;t) = 6Dt + \sum_{p=1}^{\infty} \frac{4\langle R^2 \rangle}{p^2\pi^2} \cos\left(\frac{p\pi s}{L}\right)^2 [1 - \exp(-tp^2/\tau_d)] \tag{21}$$

where the sum is over all normal modes p and τ_d denotes the longest or disengagement time. Interestingly enough, the form of eq 21 describing the msd of the primitive path points (*and not of chain segments*) according to the reptation theory is identical to the form of eq 9 discussed in previous section describing the msd of chain segments according to the Rouse model. For small times ($t < \tau_d$), $\phi(s,s;t)$ is dominated by the terms with large p. In such a case, by replacing $\cos^2(p\pi s/L)$ by its average value $^1/_2$ and converting the sum into an integral simplifies eq 21 to

$$\phi(s,s;t) = 6Dt + \int_0^\infty \mathrm{d}p \frac{4La}{p^2\pi^2} \frac{1}{2}(1 - \exp(-tp^2/\tau_d)) = 6Dt + 2\left(\frac{3}{\pi}\langle R^2 \rangle D\right)^{1/2} t^{1/2} \tag{22}$$

In contrast to the msd of *primitive path points* whose time evolution according to the reptation theory is very similar to that of chain segments according to the Rouse model, the msd of *chain segments* according to the reptation model is much more complicated: if the *segmental* $\phi(n,t)$ vs t curve is plotted on a log−log plot, reptation theory predicts four distinct regions exhibiting the following scalings: For times $t < \tau_e$ (the time at which the segmental displacement becomes comparable to the tube diameter), $\phi(n,t) \sim t^{1/2}$. In the time domain $\tau_e < t < \tau_R$, $\phi(n,t) \sim t^{1/4}$. This specific scaling behavior is predicted from the reptation theory to be a consequence of two effects, the Rouse-like diffusion and the tube constraints. For times in the region $\tau_R < t < \tau_d$, the behavior of $\phi(n,t)$ agrees with that predicted by the primitive chain dynamics and $\phi(n,t) \sim t^{1/2}$. Finally in the long time region ($t > \tau_d$), the dynamics is governed by the overall diffusion of the chain and $\phi(n,t) \sim t^1$.

Equation 22 offers us a nice way of mapping atomistic MD trajectories uniquely onto the reptation model, through a self-consistent calculation of the parameter ξ. First, a value of ξ is chosen and the mapping from the atomistic chains onto their primitive paths is carried out by implementing the procedure described by Kröger et al.[40] Then eq 20 is used to calculate $\phi(s,s;t)$ for the primitive path points, averaged over all s values. For times $t < \tau_d$, the resulting curve is compared to that obtained from eq 22, using the values of $\langle R^2 \rangle$ and D (long-time diffusivity of the center of mass) calculated directly from the atomistic MD simulations. The procedure is repeated until convergence is achieved, that is until a ξ value is found for which the two curves coincide. This mapping is performed self-consistently, without any additional adjustable parameters or any experimental input, and allows extracting reliably the tube diameter α, by utilizing atomistically collected MD data only for times shorter than τ_d. Thus, the total duration of the MD simulations required is governed solely by the time needed to faithfully calculate the center-of-mass diffusion coefficient D.

With the knowledge of $\langle R^2 \rangle$, D, and α, the friction coefficient ζ is readily obtained through[2]

$$\zeta = \frac{k_B T \alpha^2}{3N\langle R^2 \rangle D} \tag{23}$$

and the zero-shear rate viscosity η_0 through

$$\eta_0 = \frac{\rho RT}{36M}\frac{\langle R^2\rangle}{D}\frac{\langle R^2\rangle}{\alpha^2}. \quad (24)$$

V. Results

A. Structure. First the equilibrium conformational properties of polymer melts simulated through atomistic MD are compared against those obtained from the EBMC runs. Table 1a,b presents this comparison for the mean square end-to-end distance $\langle R^2\rangle$ of the melt chains and their mean square radius of gyration $\langle R_g^2\rangle$ for all systems studied here. Also shown in the table are the results obtained from MC sampling of isolated continuous unperturbed chains (CUCs).[38] The agreement between the three sets of data for both $\langle R^2\rangle$ and $\langle R_g^2\rangle$ is clear.

B. Self-Diffusion Coefficient. Figure 1a shows the msd of the chain centers of mass, $\langle (R_{cm}(t) - R_{cm}(0))^2\rangle$, for the C_{156}, C_{200}, and C_{250} systems. From the linear part of these curves, the self-diffusion coefficient D can be obtained through the Einstein relation:

$$D = \lim_{t\to\infty}\frac{\langle (R_{cm}(t) - R_{cm}(0))^2\rangle}{6t}. \quad (25)$$

To make sure that the results are free of any finite-system size effects, the longest system simulated here (C_{250}) was further simulated in two other system sizes, including 10 and 20 chains, respectively. Results for the msd of the chains centers-of-mass in the three systems are reported in Figure 1b in a log−log plot. The figure shows that the smallest 10-chain C_{250} melt suffers from significant system size effects and large statistical noise which renders any estimation of the self-diffusion coefficient problematic. In contrast, the corresponding msd curves obtained with the 16- and 20-chain systems are much smoother and (most importantly) yield the same self-diffusion coefficients: in the Einstein regime where the slope of the logarithm of the msd vs the logarithm of time equals 1, the diffusivities extracted from both systems are identical. The same conclusion was drawn by comparing the structural and conformational properties of the C_{250} chains from EBMC simulations in the three systems.[38] Consequently, for the systems studied here, all *NVT* MD simulation results reported (except, of course, for the 10-chain C_{250} melt) are definitely free of any imaging effects.

Figure 2 presents predictions for the self-diffusion coefficient D as a function of mean chain length N. Also shown in the figure are values of D obtained from past *NVT* MD simulations of systems with molecular length C_{24}−C_{117}.[19] Three distinct regions appear in the figure: (a) First is a small-M, alkane-like behavior ($N < 60$), where D follows a power-law dependence $D \sim M^{-b}$, with $b > 1$. In this regime, chain end effects, which can be described through a free volume theory,[41,42] dominate system dynamics. (b) Second is an intermediate, Rouse-like regime (from $N = 60$−70 up to $N = 156$) where $b \approx 1$.[19] (c) Third is a long chain-length, reptation-like regime ($N > 156$), where chain diffusivity exhibits a dramatic slow and $b \approx 2.4$. According to the original formulation of reptation theory, the latter exponent should be 2. Phenomena such as contour length fluctuations (CLF) and constraint release (CR) typically accelerate the escape of the chain from the tube, causing an increase in D and a decrease in η_0. Thus, a recently proposed theory that incorporates CLF and CR phenomena predicts a stronger exponent, between −2.2 and −2.3.[43] These theoretical values as well as the predictions of the present MD simulation studies are seen to be in excellent agreement with the recent experimental results of Lodge and co-workers[44] for hydrogenated polybutadiene melts, which suggest an exponent between −2.2 and −2.4. As was nicely demonstrated in this seminal work,[44] such an exponent is also consistent with experimental data reported in the past by other groups[45−47] for the dependence of D on M not only for

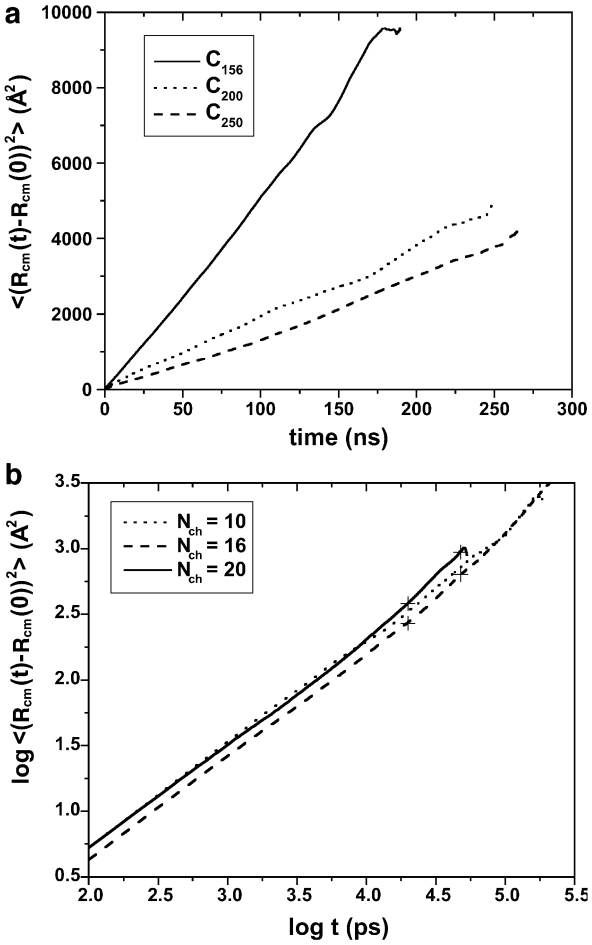

Figure 1. (a) Mean-square displacement (msd) of the chain center-of-mass for the C_{156} (solid), C_{200} (dot) and C_{250} (dashed) PE melt systems. (b) Dependence of the chain center-of-mass msd on system size for the C_{250} PE melt system. The Einstein regime (slope equal to 1) from which the self-diffusion coefficient is extracted is marked by the crosses (T = 450 K, P = 1 atm).

Table 1. Observed Values for the Equilibrium Chain for the C_{156}, C_{180}, C_{200}, and C_{250} PE Melts (T = 450 K, P = 1 atm)

a. Mean-Square End-to-End Distance

	$\langle R^2\rangle$ (Å^2)			
	C_{156}	C_{180}	C_{200}	C_{250}
MD	3000 ± 100	3500 ± 100	4000 ± 100	4850 ± 100
EBMC	3000 ± 100	3450 ± 100	4100 ± 100	4800 ± 100
CUC	3000	3400	4000	4800

b. Radius of Gyration

	$\langle R_g^2\rangle$ (Å^2)			
	C_{156}	C_{180}	C_{200}	C_{250}
MD	510 ± 25	590 ± 30	650 ± 20	810 ± 20
EBMC	510 ± 20	580 ± 20	640 ± 20	805 ± 20
CUC	500	590	650	810

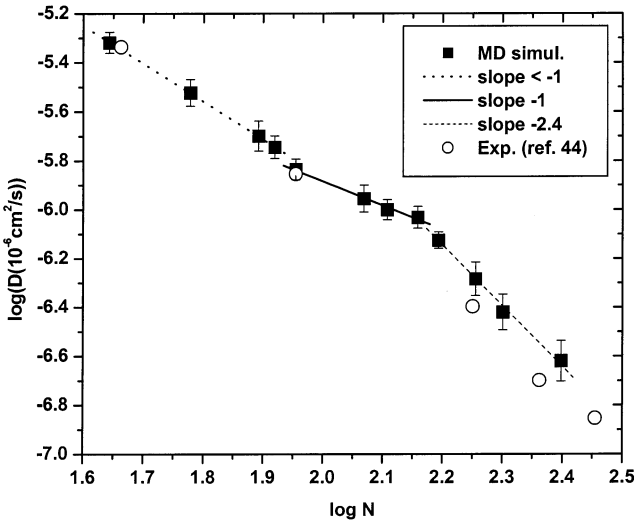

Figure 2. Predicted and experimental self-diffusion coefficients D vs chain length N in a log−log plot ($T = 450$ K, $P = 1$ atm).

hydrogenated polybutadiene melts but also for six other entangled polymer melts.

C. Dynamic Structure Factor. Parts a−d of Figure 3 present results for the intermediate dynamic structure factor for various values of the scattering vector q (0.04, 0.12, 0.20, 0.28, and 0.36 Å^{-1}) as obtained directly from the MD simulation by using eq 13 (symbols) for the four systems studied in this work: C_{78}, C_{156}, C_{200}, and C_{250}, respectively. The data for the C_{78} system have been obtained in previous MD simulations.[19] Also presented in the figures are the predictions of eq 16 using either the finite Rouse model (solid lines) or the semiflexible chain model that incorporates chain stiffness (dashed lines) for these systems.[4] The number of statistically independent segments N_k and the statistical segment length b_k entering these expressions were calculated from the MD simulation data using $N_k b_k^2 = \langle R^2 \rangle$ and $N_k b_k = L_c$ where L_c is the contour length of the chain.[38]

On the basis of our earlier investigations of the zero-shear rate viscosity, diffusion coefficient, normal-mode analysis, and friction coefficient, the C_{78} PE melt follows relatively well the Rouse dyamics,[19] at least at the length scale of the chain end-to-end distance. The plots of the single-chain dynamic structure factor presented in Figure 3a provide a further confirmation of this behavior, for wave vectors whose length q is below about 0.20 Å^{-1}. For higher q values, our atomistic MD data show $S'(q,t)$ to decay significantly slower than what is required by the Rouse model, almost for all times. In this case, by accounting for rigidity effects, the semiflexible chain model of Harnau et al.[4] improves the agreement with simulation data, particularly at shorter times. For much longer times the predictions from the semiflexible chain model and the Rouse model are indistinguishable. In general, it is confirmed that stiffness corrections to the chain motion are not enough to fully account for the slowing down of the relaxation at intermediate and longer times observed in our MD simulations. Similar conclusions have recently been drawn experimentally based on $S'(q,t)$ data collected in polybutadiene[48] and polyisobutylene[49] melts.

For the three other PE systems studied, the situation is different. For the C_{156}, C_{200}, and C_{250} melts, systematic deviations are clearly observed in the entire regime of wavevector lengths q studied, particularly at higher q values. For example, for the C_{156} PE melt, there is no q value in the interval (0.04−0.4 Å^{-1}) for which any agreement with the Rouse model can be established.

Comparatively, the dependence of the time decay of the single-chain dynamic structure factor $S(q,t)$ on chain length is shown in Figure 4. The figure presents $S(q,t)$ vs t curves at two q values (0.12 and 0.28 Å^{-1}) for all chain lengths studied here (symbols), together with the corresponding Rouse model predictions (continuous lines). That deviations from the standard Rouse behavior build up for the longer chain length systems C_{156}, C_{200}, and C_{250} at all times (particularly in the $q = 0.28$ Å^{-1} case) is evident.

In the literature, an expression for the decay of $S(q,t)$ with time based on the reptation model is given by de Gennes[15] which, however, is valid only for q values such that $1/\sqrt{\langle R^2 \rangle} \ll q/2\pi \ll 1/\alpha$. Unfortunately, for the melts studied here, the two limits $1/\sqrt{\langle R^2 \rangle}$ and $1/\alpha$ are of the same order of magnitude, which renders the use of de Gennes' formula inapplicable. To overcome the limitation, we have embarked on a new project where atomistic MD simulations with the MTS algorithm employed here are executed on significantly longer (and larger) model PE melts such as C_{1000} for times on the order of a few hundreds of nanoseconds. Results from these very promising simulations will be presented in a forthcoming publication.

D. Mean-Square Displacement of Chain Segments. We discuss next the curves obtained by monitoring the msd of atomistic chain segments with time. Mean-square displacements reported here have been calculated by monitoring the evolution with time of only the innermost segments along the chain, which are free of any chain end effects.[42] What is reported here is segmental msd plots calculated through

$$g(t) = \frac{1}{2n+1} \sum_{i=N/2-n}^{N/2+n} (\mathbf{R}(i,t) - \mathbf{R}(i,0))^2 \qquad (26)$$

with the value of the parameter n quantifying the number of innermost segments monitored being equal to four (i.e., only the dynamics of the nine most inner segments in any chain in the system is tracked).

Figure 5 shows logarithmic plots of the function $g(t)$, for various chain lengths. Four different curves are displayed in the Figure. The dashed one refers to the C_{78} PE melt and is clearly seen to obey the scaling laws predicted by the Rouse model: a short time behavior where $\phi(n,t) \sim t^{1/2}$ and the long time (Fickian diffusion) behavior where $\phi(n,t) \sim t$.[1] In fact, due to the non-negligible contribution of the linear term in eq 9 in this time scale, the slope of the short-time part of the curve is slightly higher than 0.5, close to 0.6. It is also interesting that the end of this short-time behavior appears at $t \approx 2$ ns, which is practically the Rouse time of the C_{78} melt.[19]

Also shown in Figure are the curves corresponding to the C_{156} (dotted), the C_{200} (long-dashed), and the C_{250} (solid) PE melts. Although the first two curves do not exhibit any pronounced structure, the curve corresponding to the C_{250} PE melt shows three distinct breaks (marked by the arrows) characteristic of a system undergoing a transition from a Rouse- to a reptation-like dynamics. The corresponding exponents quantifying the scaling of $\phi(n,t)$ with t are equal to 0.55, 0.40, 0.60, and 0.85, respectively. These are not exactly the same

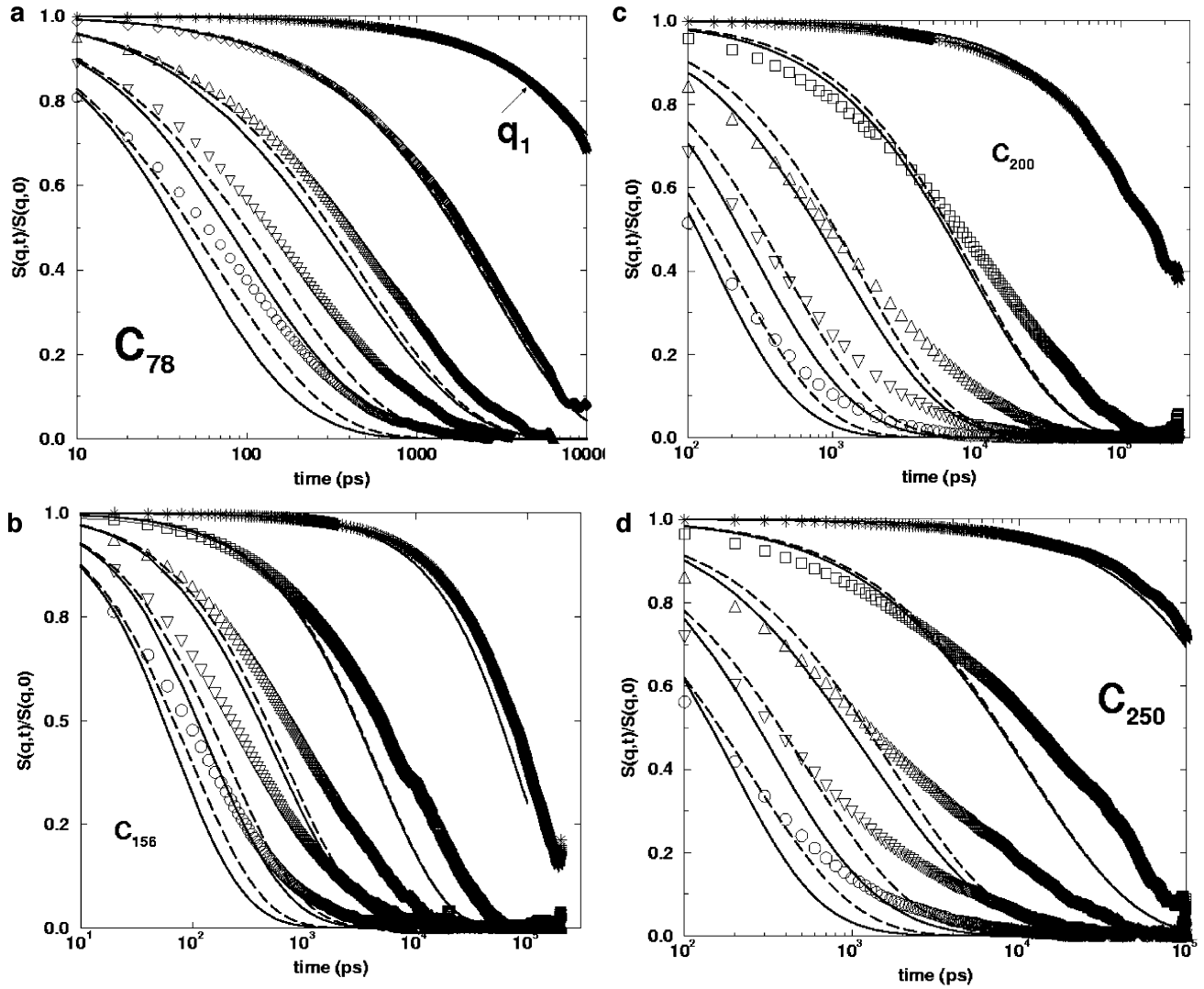

Figure 3. Normalized single-chain dynamic structure factor $S(q,t)/S(q,0)$ obtained from the MD simulations (symbols) for various q values (0.04, 0.12, 0.20, 0.28, and 0.36 Å^{-1}) for different molecular weights, (a) C_{78}, (b) C_{156}, (c) C_{200}, and (d) C_{250}. With the solid lines are the predictions from the Rouse model and with the dashed those from the Harnau et al. model ($q_1 = 0.04$ Å^{-1}).

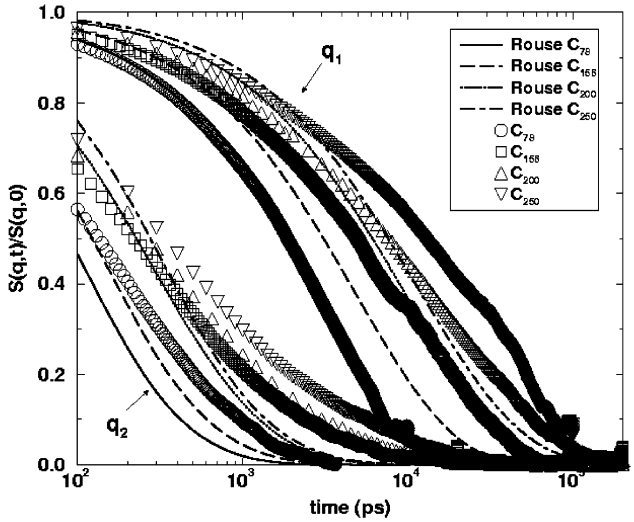

Figure 4. $S(q,t)/S(q,0)$ values for the systems discussed in Figure 3, parts a−d, and for two q values ($q_1 = 0.12$ Å^{-1} and $q_2 = 0.28$ Å^{-1}).

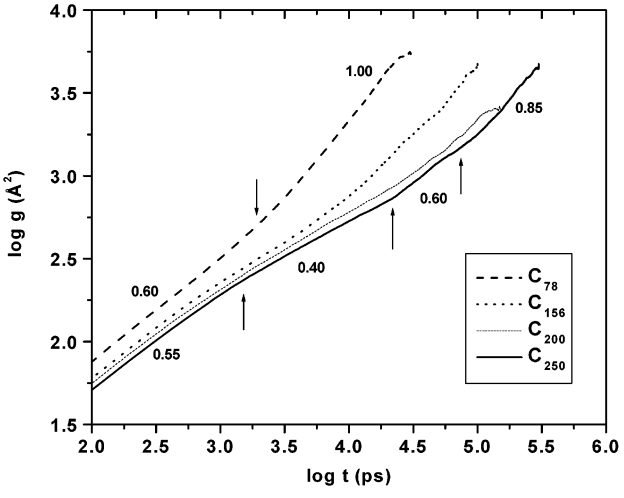

Figure 5. Mean-square displacement $g(t)$ of the innermost atomistic chain segments vs time t in a log−log plot for the PE melt systems studied here.

with those predicted by the reptation theory (equal to 0.50, 0.25, 0.50, and 1.00, respectively). The largest deviation is observed for the exponent of the power-law in the intermediate regime due to the simultaneous effect of the Rouse diffusion and tube constraints on the segmental dynamics. However, it should be kept in mind that C_{250} is a rather short-chain system for which

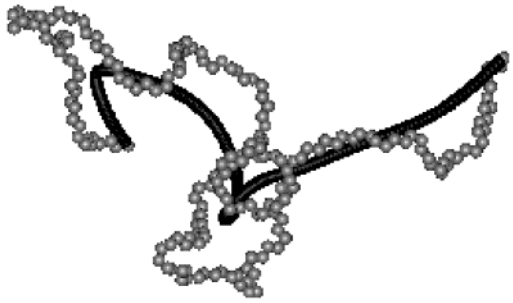

Figure 6. An atomistic snapshot of a C_{200} PE melt chain (gray beads) and its corresponding primitive path (smoother curve) obtained for $\xi = 50$.

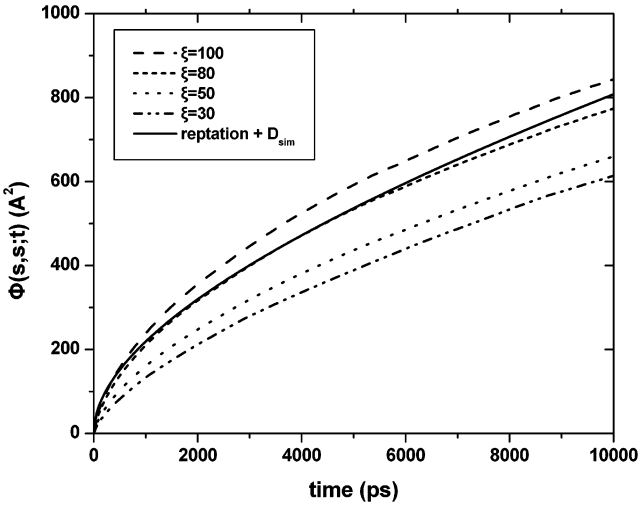

Figure 7. Mean-square displacement of the primitive path segments $\phi(s,s;t)$ vs time, averaged over s, as predicted from mapping the atomistic MD data onto the reptation theory, eq 20, using various values of the parameter ξ determining the entanglement spacing. The solid curve corresponds to the prediction of the pure reptation theory, eq 22, using the values of D and $\langle R^2 \rangle$ obtained directly from the MD simulations.

reptation theory should only be marginally applicable. In the literature, simulations with coarse-grained models have shown that as the chain length increases, the corresponding exponent decreases, gradually approaching the $^1/_4$ value.[23,29] Atomistic simulations with longer PE melt chains are clearly needed in order to clarify this, and such a work is already in progress.

E. Friction Factor: Zero-Shear Rate Viscosity. According to the Rouse model, the friction factor ζ and the zero-shear rate viscosity η_0 can be calculated directly from D through eqs 6 and 7. In contrast, the use of the reptation theory equations, eqs 23 and 24, respectively, requires the calculation of the tube diameter α, through the procedure described in section IVB. A typical projection of an atomistic chain (from the C_{200} system) onto its primitive path is shown in Figure 6.

Typical curves of the mean-square displacement of the primitive path points $\phi(s,s;t)$ for the C_{200} PE melt as a function of time t are shown in Figure 7. It is seen that the value of ξ which provides a consistent mapping of the atomistic MD data onto the reptation theory is $\xi = 80 \pm 5$. For this value, the tube diameter α is calculated to be $\alpha \sim 60$ Å. Exactly the same α value is obtained by mapping the C_{250} melt chains onto their primitive paths. This value is larger than that extracted from rheological experiments with high molecular weight PE melts, which is around 34−40 Å.[2,12,20] The main reason for this is that the value of α is actually different for the

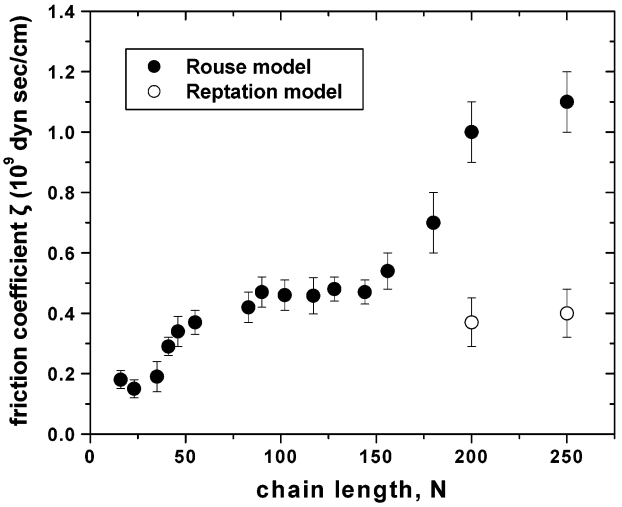

Figure 8. Monomer friction coefficient ζ vs chain length N, obtained from mapping the atomistic MD data onto the Rouse (filled circles) or the reptation model (open circles).

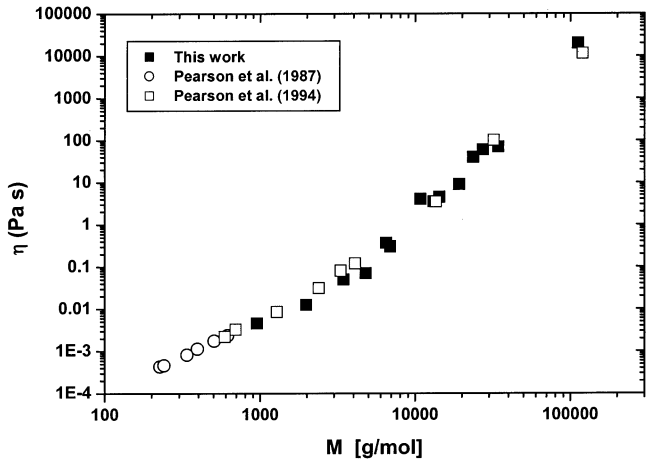

Figure 9. Measured zero-shear rate viscosity η_0 values vs weight-average molecular weight M.

relatively short PE systems investigated in this work (C_{200} and C_{250}) than for long-chain PE, as pointed out by Richter et al.[12] In contrast, for the shorter C_{180}, C_{156}, and C_{78} systems, no physical value of α could be identified for which a consistent mapping of the atomistic MD data onto the reptation model is achieved.

Figure 8 shows results for the monomeric friction factor ζ as a function of the mean chain length N, over the entire range of molecular lengths studied. Filled circles depict results obtained from mapping the atomistic MD data onto the Rouse model, whereas open circles depict results obtained from mapping the atomistic MD data onto the reptation model. According to its definition, ζ should be independent of chain length, its value being determined solely by the chemical constitution of the melt. The figure shows clearly that, at around C_{156}, a change in the mechanism of the dynamics takes place, which cannot be accommodated by the Rouse model unless a chain-length dependent ζ value is assumed. In contrast, in this regime ($N > 156$), the reptation model provides a consistent description of the system dynamics characterized by a constant [0.4×10^{-9} (dyn s)/cm], chain-length independent ζ value per methylene or methyl segment.

Figure 9 depicts the experimentally obtained zero shear viscosity as a function of the weight-average

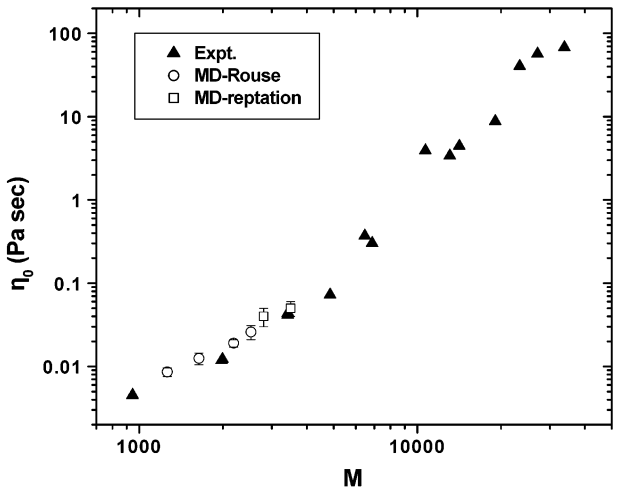

Figure 10. Zero-shear rate viscosity η_0 vs chain length N, obtained from mapping atomistic MD data onto the Rouse model for the smaller chain lengths (circles), and onto the reptation model for the higher chain lengths (squares). Also shown in the figure are experimentally obtained η_0 values (triangles).

molecular weight M.[50] It is clear that the two regions, the Rouse and the reptation, are unambiguously distinguished, and that the data conform to the respective scalings of 1 and 3.4. The intersection of the slopes defines the critical molecular weight $M_c \approx 2500$, from which the entanglement molecular weight $M_e \approx 1250$ is extracted. This value is in excellent agreement with reported literature values.[1,45] Some scattering in the data, especially in the high-M region is attributed to uncertainties in the M and η_0 (fitting procedure) determination. For comparison, also shown in Figure 9 are the corresponding experimental data of Pearson et al.[45] obtained with model *n*-alkane and linear PE samples. The agreement between the two sets of data is excellent throughout the molecular weight range. Some discrepancies observed in a few samples may relate to the uncertainties discussed already. Note that the Pearson et al. data were reported at 175 °C and had to be translated to 180 °C by utilizing values of the apparent activation energies for viscous flow.

Figure 10 presents the zero-shear rate viscosity η_0 as a function of the molecular weight for all the systems studied here. For the systems smaller than C_{156} the Rouse model, eq 7, was used, whereas for the longer systems the reptation formula, eq 24, was used. Also reported in the figure are the experimentally measured η_0 values. The η_0 values were obtained from the reptation model using the value for the entanglement spacing $\alpha = 60$ Å determined above. The agreement of the simulation results with the experimental ones is remarkable for all systems studied.

At this point it is worth mentioning that if the viscosities of the two longer chains (C_{200} and C_{250}) were calculated by the Rouse model (eq 7), they would also lie close to the experimental data. However, they would correspond to values of the monomer friction coefficient ζ different from those dictated by the Rouse model in its regime of validity (chain lengths between C_{80} and C_{150}, approximately), which would render the mapping not self-consistent.

VI. Conclusions: Future Plans

We have presented results from very long (up to 300 ns) equilibrium atomistic MD simulations with model PE melt systems of molecular lengths ranging from C_{24} up to C_{250}. A dramatic slow of the self-diffusion coefficient D was observed when the molecular length of the polymer exceeded C_{156}. For $N > 156$, the power-law exponent quantifying the dependence of D on N was found to be stronger than that predicted from the Rouse model, and in very good agreement with a recently proposed reptation theory, which incorporates contour length fluctuations and constrained release mechanisms.[43] It also agrees very well with recently measured experimental data.[44]

Results have also been presented concerning the single chain dynamic structure factor $S(q,t)$ for various q values and all four (C_{78}, C_{156}, C_{200}, and C_{250}) PE melt systems studied. C_{78} was seen to follow the analytical $S(q,t)$ predictions of the Rouse model quite well for q values smaller than about 0.2 Å^{-1}; higher q values, which correspond to the dynamics of shorter-length scale chain segments, were seen to deviate from the Rouse behavior. That C_{78} is a melt that follows Rouse dynamics quite faithfully was further confirmed by observing the scaling of the segmental msd with time on a log−log plot. On the other hand, the corresponding msd vs time curves (again on a log−log plot) for the longer C_{250} PE melt demonstrated its dynamics to be more reptation- than Rouse-like: three distinct breaks were observed in the curve, with scalings indicative of reptation.

We have also presented a consistent way of mapping the atomistic MD data onto the Rouse and the reptation molecular models. The latter mapping involved an intermediate projection step of the atomistically detailed chains onto primitive paths.[40] The Rouse model was seen to produce consistent (chain-length independent) results for the monomer friction factor ζ only in the interval of chain lengths $70 < N < 156$. For chain lengths $N > 156$, only the reptation model was capable of producing consistent results for ζ. The tube diameter α was estimated to be about 60 Å. The zero-shear rate viscosity η_0 was also calculated, using the Rouse model for the shorter systems and the reptation theory for the longer ones. η_0 values extracted from the simulations were seen to agree remarkably well with recently obtained experimental η_0 measurements on model linear PE melts.

The present study focused on the estimation of the diffusion and rheological properties of PE melts of length up to C_{250}. Earlier works had addressed the transport and dynamic properties of *n*-alkanes and of shorter PE melts, of length up to C_{120}. The dynamic and rheological properties of these melts were obtained by two different approaches[51,19,39] and gave identical results. Future plans include the atomistic simulation of even longer PE melt systems (ranging in molecular length from C_{400} to C_{1000}) and a direct comparison of the MD simulation findings with NSE and double-quantum nuclear magnetic resonance (DQ NMR) experiments.

Acknowledgment. V.A.H. would like to acknowledge the support of the European Commission through TMR Grant No. ERB FMGE CT950051 (the TRACS Program at EPCC).

Appendix: Time Correlation Function $\phi(n,m;t)$ for the Finite Rouse Model

The normal coordinates for the finite Rouse model, are given as a function of the position vectors of the segments by[19]

$$\mathbf{X}_p(t) = \sum_{j=1}^{N} \sqrt{\frac{2-\delta_{p0}}{N}} \cos\left(\frac{(j-{}^1/_2)p\pi}{N}\right) \mathbf{R}_{j-1}(t) \qquad \text{(A.1)}$$

with $j = 1, 2, ..., N$ and $p = 0, 1, ..., N-1$, and $\mathbf{R}_j(t)$ denoting the position vector of bead j at time t. Through a back-transformation

$$\mathbf{R}_j(t) = \sum_{p=0}^{N-1} \sqrt{\frac{2-\delta_{p0}}{N}} \cos\left(\frac{(j-{}^1/_2)p\pi}{N}\right) \mathbf{X}_p(t) \quad \text{(A.2)}$$

The time autocorrelation function of the normal modes is given by the expression

$$\langle \mathbf{X}_p(t) \cdot \mathbf{X}_p(0) \rangle = 3\frac{k_B T}{k_p} \exp\left(-\frac{t}{\tau_p}\right) = \frac{b_k^2}{4 \sin^2\left(\frac{p\pi}{2N}\right)} \exp\left(-\frac{t}{\tau_p}\right) \quad \text{(A.3)}$$

In particular, for the zero normal mode and by using Einstein's relation

$$\left\langle \left(\sqrt{\frac{1}{N}} (\mathbf{X}_o(t) - \mathbf{X}_o(0)) \right)^2 \right\rangle = \langle ((\mathbf{R}_{cm}(t) - \mathbf{R}_{cm}(0)))^2 \rangle = 6Dt \quad \text{(A.4)}$$

To calculate the time correlation function $\phi(n,m;t)$, we follow the same procedure as for the continuous Rouse model described in ref 2, appendix 4.III, and we find that

$$\phi(n,m;t) = \left\langle \left[\sqrt{\frac{1}{N_k}} (\mathbf{X}_o(t) - \mathbf{X}_o(0)) + \sum_{p=1}^{N_k-1} \sqrt{\frac{2}{N_k}} \left(\cos\left(\frac{p\pi(n-{}^1/_2)}{N_k}\right) \mathbf{X}_p(t) - \cos\left(\frac{p\pi(m-{}^1/_2)}{N_k}\right) \mathbf{X}_p(0) \right) \right]^2 \right\rangle \quad \text{(A.5)}$$

where N_k denotes the number of statistical segment lengths. By using the previous expressions, eqs A.3−A.5, we get

$$\phi(n,m;t) = 6Dt + \frac{b_k^2}{2N_k} \sum_{p=1}^{N_k-1} \frac{1}{\sin^2\left(\frac{p\pi}{2N_k}\right)} \left[\cos\left(\frac{p\pi(m-{}^1/_2)}{N_k}\right) - \cos\left(\frac{p\pi(n-{}^1/_2)}{N_k}\right) \right]^2 + \frac{b_k^2}{N_k} \sum_{p=1}^{N_k} \frac{1}{\sin^2\left(\frac{p\pi}{2N_k}\right)} \cos\left(\frac{p\pi(n-{}^1/_2)}{N_k}\right) \cos\left(\frac{p\pi(m-{}^1/_2)}{N_k}\right) \left[1 - \exp\left(-\frac{t}{\tau_p}\right) \right] \quad \text{(A.6)}$$

References and Notes

(1) Ferry, J. D. *Viscoelastic Properties of Polymers*; J. Wiley & Sons: New York, 1980. Berry, G. C.; Fox, T. G. *Adv. Polym. Sci.* **1968**, *5*, 261.
(2) Doi, M.; Edwards, S. F. *The Theory of Polymer Dynamics*; Clarendon Press: Oxford, England, 1986.
(3) Rouse, P. E. *J. Chem. Phys.* **1953**, *21*, 1272.
(4) Harnau, L.; Winkler, R. G.; Reineker, P. *J. Chem. Phys.* **1995**, *102*, 7750; **1996**, *104*, 6355.
(5) Ronca, G. *J. Chem. Phys.* **1983**, *79*, 1031.
(6) Hess, W. *Macromolecules* **1986**, *19*, 1395; **1988**, *21*, 2620.
(7) des Cloizeau, J. *J. Phys. I (Fr.)* **1993**, *3*, 1523.
(8) Schweizer, K. S. *J. Chem. Phys.* **1989**, *91*, 5802; 5822.
(9) Perkins, T. T.; Smith, D. E.; Chu, S. *Science* **1994**, *264*, 819.
(10) Schleger, P.; Farago, B.; Lartigue, C.; Kollmar, A.; Richter, D. *Phys. Rev. Lett.* **1998**, *81*, 124.
(11) Richter, D.; Willner, L.; Zirkel, A.; Farago, B.; Fetters, L. J.; Huang, J. S. *Phys. Rev. Lett.* **1993**, *71*, 4158.
(12) Richter, D.; Willner, L.; Zirkel, A.; Farago, B.; Fetters, L. J.; Huang, J. S. *Macromolecules* **1994**, *27*, 7437.
(13) Richter, D.; Farago, B.; Fetters, L. J.; Huang, J. S.; Ewen, B.; Lartigue, C.; *Phys. Rev. Lett.* **1990**, *64*, 1389.
(14) Paul, W.; Smith, G. D.; Yoon, D. Y.; Farago, B.; Rathgeber, S.; Zirkel, A.; Willner, L.; Richter, D. *Phys. Rev. Lett.* **1998**, *80*, 2346.
(15) de Gennes, P. G. *J. Phys. (Paris)* **1981**, *42*, 735.
(16) Graft, R.; Heuer, A.; Spiess, H. W. *Phys. Rev. Lett.* **1998**, *80*, 5738.
(17) Evans, D. J.; Morris, G. P. *Statistical Mechanics of Nonequilibrium Liquids*; Academic Press: London, 1990.
(18) Mondello, M.; Grest, G. S. *J. Chem. Phys.* **1997**, *106*, 9327.
(19) Harmandaris, V. A.; Mavrantzas, V. G.; Theodorou, D. N. *Macromolecules* **1998**, *31*, 7934.
(20) Paul, W.; Smith, G. D.; Yoon, Do Y. *Macromolecules* **1997**, *30*, 7772.
(21) Padding, J. T.; Briels, W. J. *J. Chem. Phys.* **2001**, *114*, 8685; **2002**, *117*, 925.
(22) Kremer, K.; Grest, G. S. *J. Chem. Phys.* **1990**, *92*, 5057.
(23) Pütz, M.; Kremer, K.; Grest, G. S. *Europhys. Lett.* **2000**, *49*, 735.
(24) Smith, S. W.; Hall, C. K.; Freeman, B. D. *J. Chem. Phys.* **1996**, *104*, 5616.
(25) Kröger, M.; Hess, S. *Phys. Rev. Lett.* **2000**, *85*, 1128.
(26) Pakula, T.; Geyler, S. *Macromolecules* **1987**, *20*, 2909.
(27) Haire, K. R.; Carver, T. J.; Windle, A. H. *Comput. Theor. Polym. Sci.* **2001**, *11*, 17.
(28) Kreitmeier, S.; Wittkop, M.; Trautenberg, H.; Holzl, T.; Goritz, D *J. Comput. Phys.* **1997**, *133*, 181.
(29) Kreer, T.; Baschnagel, J.; Müller, M.; Binder, K *Macromolecules* **2001**, *34*, 1105.
(30) Padding, J. T.; Briels, W. J. *J. Chem. Phys.* **2001**, *115*, 2846.
(31) Dodd, L. R.; Theodorou, D. N. *Adv. Polym. Sci.* **1994**, *116*, 249.
(32) Van der Ploeg, P.; Berendsen, H. J. *J. Chem. Phys.* **1982**, *76*, 3271.
(33) Ryckaert, J. P.; Bellemans, A. *Chem. Phys. Lett.* **1975**, *30*, 123.
(34) Ryckaert, J. P.; Ciccoti, G.; Berendsen, H. J. C. *J. Comput. Phys.* **1977**, *101*, 327.
(35) Andersen, H. C. *J. Comput. Phys.* **1983**, *52*, 24.
(36) Tuckerman, M. E.; Berne, B. J.; Martyna, G. J. *J. Chem. Phys.* **1992**, *97*, 1990.
(37) Martyna, G. J.; Tuckerman, M. E.; Tobias, D. J.; Klein, M. L. *Mol. Phys.* **1996**, *87*, 1117.
(38) Mavrantzas, V. G.; Boone, T. D.; Zervopoulou, E.; Theodorou, D. N. *Macromolecules* **1999**, *32*, 5072; Karayiannis, N. Ch.; Mavrantzas, V. G.; Theodorou, D. N. *Phys. Rev. Lett.* **2002**, *88*, 105503−1.
(39) Harmandaris, V. A.; Mavrantzas, V. G.; Theodorou, D. N. *Macromolecules* **2000**, *33*, 8062.
(40) Kröger, M.; Ramírez, J.; Öttinger, H. C. *Polymer* **2002**, *43*, 477.
(41) Bueche, F. *Physical Properties of Polymers*; Interscience: New York, 1962.
(42) Harmandaris, V. A.; Doxastakis, M.; Mavrantzas, V. G.; Theodorou, D. N. *J. Chem. Phys.* **2002**, *116*, 436.
(43) Frischeknecht, A. L.; Milner, S. T. *Macromolecules* **2000**, *33*, 5273. Milner, S. T.; McLeish, T. C. B. *Phys. Rev. Lett.* **1998**, *81*, 725.
(44) Lodge, T. P. *Phys. Rev. Lett.* **1999**, *83*, 3218. Tao, H.; Lodge, T. P.; von Meerwall, E. D. *Macromolecules* **2000**, *33*, 1747.
(45) Pearson, D. S.; Ver Strate, G.; von Meerwall, E.; Schilling, F. C. *Macromolecules* **1987**, *20*, 1133. Pearson, D. S.; Fetters, L. J.; Graessley, W. W.; Ver Strate, G.; von Meerwall, E. *Macromolecules* **1994**, *27*, 711.
(46) Crist, B.; Green, P. F.; Jones, R. A. L.; Kramer, E. J. *Macromolecules* **1989**, *22*, 2857.

(47) von Seggern, J.; Klotz, S.; Cantow, H.-J. *Macromolecules* **1991**, *24*, 3300.
(48) Smith, G. D.; Paul, W.; Monkenbush, M.; Richter, D. *J. Chem. Phys.* **2001**, *114*, 4285.
(49) Smith, G. D.; Paul, W.; Monkenbush, M.; Willner, L.; Richter, D.; Qiou, X. H.; Ediger, M. D. *Macromolecules* **1999**, *32*, 8857.
(50) Vlassopoulos, D. Unpublished data.
(51) Mavrantzas, V. G.; Öttinger, H. C. *Macromolecules* **2002**, *35*, 960. Mavrantzas, V. G.; Theodorou, D. N. *Macromolecules* **1998**, *31*, 6310.

MA020009G